Vietnam Journal of Science and Technology ***56*** *(2) (2018) 174-183*

DOI: 10.15625/2525-2518/56/2/10599

A STUDY ON THE LOCALIZED CORROSION INHIBITION FOR MILD STEEL IN SALINE SOLUTION

Nguyen Dang Nam[1, *], Nguyen To Hoai[2], Pham Van Hien[3]

[1]*Institute for Basic and Applied Research, Duy Tan University, 3 Quang Trung, Da Nang City 550000, Viet Nam*
[2]*PetroVietnam University, 762 Cach Mang Thang Tam Street, Long Toan Ward, Ba Ria City 790000, Viet Nam*
[3]*Faculty of Chemical Engineering, Bach Khoa University, VNU-HCM, 268 Ly Thuong Kiet Street, District 10, Ho Chi Minh City 700000, Viet Nam*

[*]Email: *ndnam12a18@gmail.com*

Received: 7 August 2017; Accepted for publication: 5 March 2018

Abstract. In this study, 0.45 mM yttrium 4-nitrocinnamate ($Y(4NO_2Cin)_3$) embedded in various aqueous chloride solutions, which has been studied as a possible localized corrosion inhibition system using electrochemical techniques and surface analysis. Furthermore, a wire-beam electrode (WBE) exposed to NaCl solutions containing $Y(4NO_2Cin)_3$ compound. The results indicated the possible application of a WBE in simulating and monitoring the localized corrosion inhibition. Moreover, $Y(4NO_2Cin)_3$ compound showed an excellent localized corrosion inhibition at 0.01 M due to high inhibition performance and good protective film formation. It also indicated that addition of 0.45 mM $Y(4NO_2Cin)_3$ compound increased the localized corrosion inhibition with a decrease of the Cl^- ion concentration in the investigated solutions. A new method of localized corrosion inhibition estimation has been developed using a WBE which shows a consistent result with electrochemical and surface analysis data. In addition, other electrochemical techniques and surface analysis are also used for not only ensuring but also confirming the localized corrosion inhibition.

Keywords: mild steel, localized corrosion inhibition, electrochemical techniques, surface analysis, wire beam electrode.

Classification numbers: 2.5.1; 2.5.3; 2.10.3;

1. INTRODUCTION

Mild steel is most widely used in various industrial applications such as oil and gas, chemical plants and water treatment due to the low cost and high strength [1]. However, in case of practical applications, it is totally a different scenario which should face a poor corrosion resistance in all kinds of aggressive environments such as industrial cleaning, acid corrosion in the acid picking processes, acid rain, and oil well acidification, as well as ocean environment [2, 3]. Therefore, many attempts have been recommended for mitigating the steel corrosion using

the control of its microstructure [4], coatings [5], surface treatments [6], adding certain alloying elements [7], and self-assembly of organic molecules on a solid surface or at the solid–liquid interface [8], as well as the corrosion inhibitors [9-13]. Among these methods, addition of corrosion inhibitor to the environment has been tremendously used as the ideal way for improving corrosion resistance of steel due to the cost savings, easy to use, and not interrupting any processes. Consequently, many studies have been investigated the corrosion inhibitions and its mechanism in steels [9-13]. Chromates and molybdates are widely used as corrosion inhibitors due to the effective corrosion protection. However, they pollute the environment and are also hazardous to human health and might cause cancer, particularly chromate-based inhibitors [14, 15]. Therefore, it needs more effective inhibitors, which is environmentally friendly and ecologically acceptable, arising the requirement to develop the new generation corrosion inhibitors which can be suitably used in combating corrosion and replace chromate and molybdate technologies. Imidazoline and its derivatives have been typically recommended as the suitable candidates for replacing chromate and molybdate technologies due to their high effective corrosion inhibition. However, the localized corrosion inhibition of these compounds is still questionable, since a small number of minor anodes and major cathodes have been formed on the steel surfaces immersed in inhibited systems containing these compounds, resulting in the localized corrosion [16]. Thus, the localized corrosion inhibition systems need to be developed further, more efficiently, and environmentally friendly.

Currently, our work is on rare earth organic compounds, some of which have been shown the superior protective corrosion of steel over a longer period. We have recently developed the new yttrium 4-nitrocinnamate - $Y(4NO_2Cin)_3$ - to replace chromate, molybdate, imidazoline and its derivative technologies [17-19]. While corrosion inhibition itself is not new, there has been little study on inhibitor properties using new electrochemical techniques such as the wire beam electrode to measure and evaluate the information regarding localized corrosion inhibition. Understanding and managing localized corrosion will be critical to improve the lifetime of steel in the aggressive environments. Therefore, this work further extends the study of the corrosion and localized corrosion inhibition mechanism by which the $Y(4NO_2Cin)_3$ compound mitigates steel corrosion and localized corrosion [17]. A combination of aggressive environments dependent potentiodynamic polarization (PD), electrochemical impedance spectroscopy (EIS), and wire beam electrode (WBE) has been utilized to correlate the inhibition performance response with the surface characterizations.

2. EXPERIMENTAL

The details of the synthesis and characterization of $Y(4NO_2Cin)_3$ compound as an investigated corrosion inhibitor in this study can be found in the previous publication [17, 20]. 0.45 mM $Y(4\text{-}NO_2Cin)_3$ was added to 0.01, 0.10, and 0.60 M NaCl solutions in distilled water using reagent grade sodium chloride purchased from Sigma Aldrich with 12 hours of stirring. The steel used as working electrodes and coupons were fabricated from sheet as 1 cm × 1 cm × 0.3 cm for the electrochemical measurements and surface analysis. The exposed area of these specimens was 1 cm^2 and was finished by grinding with 1200-grit silicon carbide paper. Three electrode system including a steel specimen, a titanium, and a saturated calomel electrode as the working, counter, and reference electrodes was used for electrochemical measurements. After immersion of the sample for 10 h in the naturally-aerated solution with and without inhibitor addition, the EIS and PD were performed using a VSP system with a commercial software program for AC measurements. The frequency of EIS tests ranged from 10 kHz to 10 mHz using

the 10 mV of peak to peak amplitude of the sinusoidal perturbation. Potentiodynamic polarization tests were carried out at a rate of 0.166 mV/s ranging from an initial potential of -250 mV vs. E_{corr} to 0 mV_{SCE} of anodic potential. The WBE was made from one hundred identical steel wires embedded in epoxy resin, insulated from each other with a thin epoxy layer for investigating the trend of localized corrosion and inhibition of steel in the investigated solutions. The diameter of each wire is 0.19 cm and acted as a sensor and simulated as a corrosion substrate. The WBE surface was ground by 100, 600, and 1200-grit silicon carbide papers, then rinsed with deionized water and ethanol before being performed in three liters of solution. $Y(4NO_2Cin)_3$ compound was injected into the testing cell after a 30 min period of initial corrosion testing and measured after 10 h of immersion time. The mapping galvanic currents between a chosen wire and all the other wires sorted together using a pre-programmed Auto switch device and an ACM Auto ZRA indicated the corrosion processes. The galvanic current data were performed and characterized using procedures like that described in a previous publication [17]. To investigate the relationship between the electrochemical properties and surface morphology, the specimens were examined by scanning electron microscopy (SEM) and attenuated total reflectance Fourier transform infrared spectroscopy (ATR-FTIR, Alpha-FTIR spectrometer) after immersion for 10 h in solutions at room temperature.

3. RESULTS AND DISCUSSION

Figure 1 indicates the EIS results in the Nyquist and Bode formats obtained from the mild steel immersed in different NaCl concentration solutions after 10 h of immersion time.

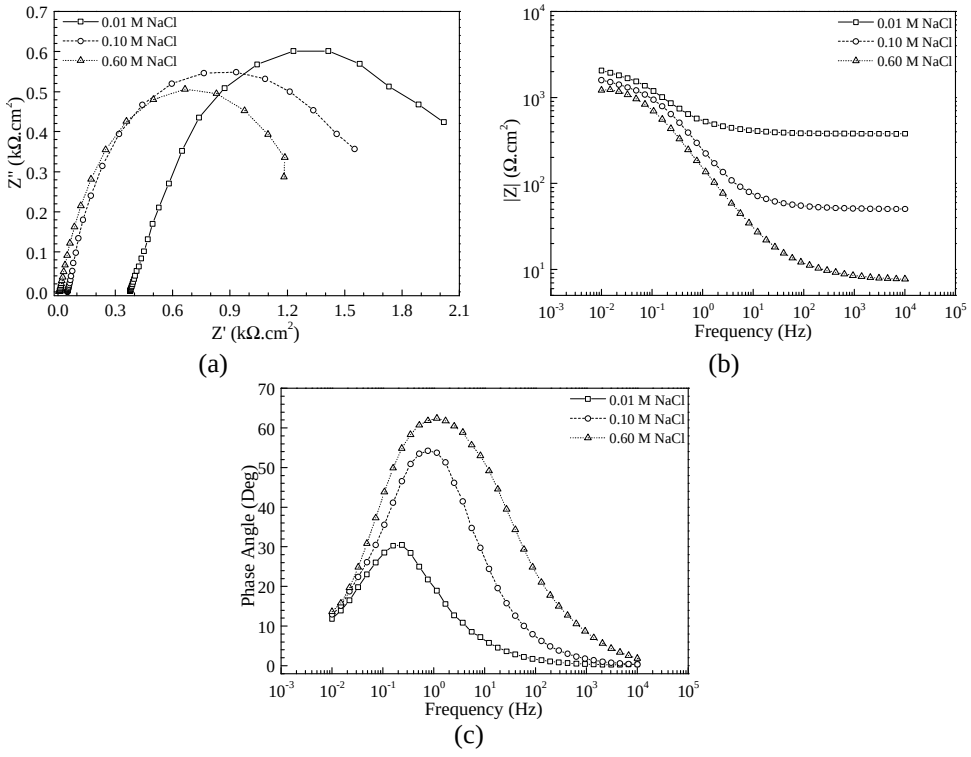

Figure 1. EIS results of mild steel after 10 h immersion in (a) 0.01, (b) 0.10, and (c) 0.60 M NaCl solutions.

Figure 1(a) shows the impedance spectra in the form of the Nyquist plots, additionally, Fig. 1(b and c) presents the Bode plots (impedance and phase angle vs. frequency). The results clearly show that the impedance value increased with a decrease in NaCl concentration. Whereas, solution resistance decreased with a decrease in NaCl concentration, indicating that NaCl could decrease the resistance of the solution. In addition, the radius and the size of the capacitive loops were much changed with chloride-contained solutions, indicating that the electrochemical behavior of mild steel has been strongly affected by Cl^- concentration. The equivalent electrical circuits were shown in Fig. 2(d) and were employed to fit the EIS of the mild steel in solution containing different Cl^- concentration. The equivalent circuit used to fit the EIS data displaying two capacitive loops for all specimens. The changes of the impedance spectra in both size and shape effects with the Cl^- concentration including the decrease in the capacitive loop in size, showed that the rust layer formed on the steel surface destroyed under the Cl^- erosion.

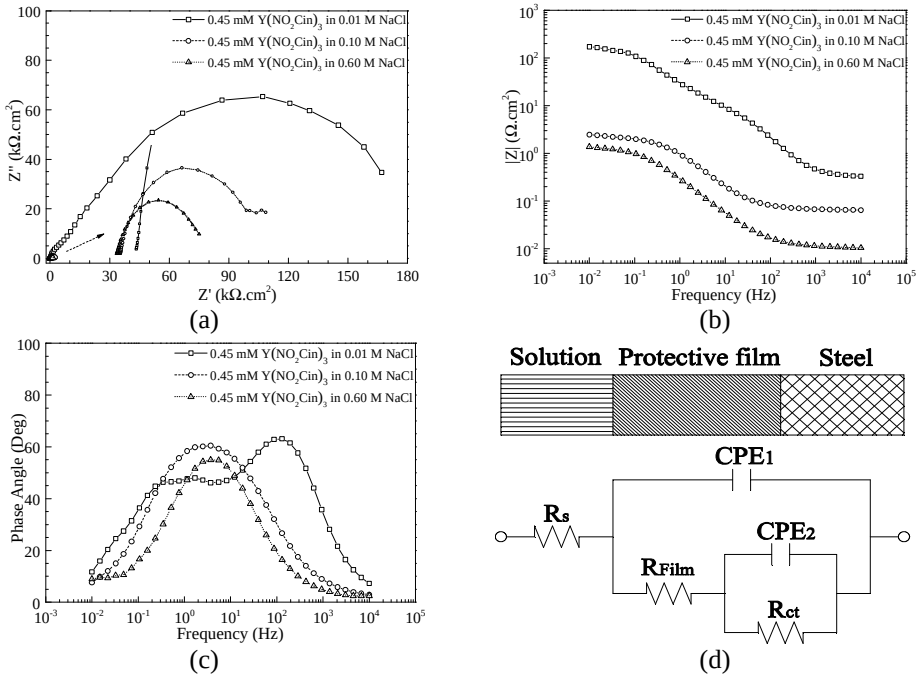

Figure 2. EIS results of mild steel after 10 h immersion in 0.45 mM $Y(4NO_2Cin)_3$ solutions containing (a) 0.01, (b) 0.10, and (c) 0.60 M NaCl, and (d) equivalent circuit for fitting the EIS data.

Table 1. Electrochemical impedance measurements of steel immersed in solutions containing different NaCl concentration without and with 0.45 mM $Y(4NO_2Cin)_3$ addition; (R_{film} is replaced by R_{rust} for uninhibited systems).

$Y(4NO_2Cin)_3$ (mM)	NaCl (M)	R_s ($\Omega.cm^2$)	CPE_{film} C ($\mu F/cm^2$)	CPE_{film} n (0~1)	R_{film} ($\Omega.cm^2$)	CPE_{dl} C ($\mu F/cm^2$)	CPE_{dl} n (0~1)	R_{ct} ($\Omega.cm^2$)
0.00	0.01	378	148	0.6905	518	198	0.7170	1828
0.45		256	2	0.9007	10800	9	0.7953	190100
0.00	0.10	50	894	0.7520	79	238	0.7720	1448
0.45		66	200	0.8028	507	66	0.7899	2194
0.00	0.60	8	618	0.8038	9	489	0.7832	1016
0.45		11	382	0.7686	363	107	0.7864	1354

Figure 2(a-c) shows the EIS results in the Nyquist and Bode formats obtained from the mild steel immersed in different NaCl concentration solutions containing 0.45 mM $Y(4NO_2Cin)_3$ after 10 h of immersion time. The results indicated that the diameter of the semicircular was increased and an improvement of a more capacitive surface film has also observed when $Y(4NO_2Cin)_3$ compound was added to the NaCl solutions, indicating the formation of the protective layer. Furthermore, the impedance and phase angles increased with adding $Y(4NO_2Cin)_3$ compound to solution and decreased with Cl^- containing solution due to the formation of surface film. This indicates that the addition of an amount of $Y(4NO_2Cin)_3$ compound improves protective film formation on the steel surface. Combination the EIS data with surface analysis including SEM and ATR-FTIR, the equivalent circuit in Figure 2(d) was recommended for fitting the EIS data using the Zsimpwin program. This equivalent circuit includes the solution resistance (R_s) of the test electrolyte between the working electrode and the reference electrode, the constant phase element CPE_{film} of the protective film/electrolyte interface, the protective film resistance R_{film} of the protective film formed on the steel surface, and the charge transfer resistance R_{ct} of the substrate/protective film (or rust) interface. The electrochemical information after fitting was given in Table 1. A significant decrease in solution resistance was obtained when NaCl concentration increased, whereas rust and charge transfer resistance strongly decreased with an increase in NaCl concentration. These values increased with a decrease in NaCl concentration, indicating the compact protective film formed on the steel surface. It also shows that the protective and double layer capacitances decreased when $Y(4NO_2Cin)_3$ compound was added to solutions and these values decreased with a decrease in $Y(4NO_2Cin)_3$ compound concentrations, indicating a more capacitive surface film. A better coverage of the surface has been reached, when $Y(4NO_2Cin)_3$ compound was added to solution containing lower NaCl concentration due to an increase in film and charge transfer resistances and a reduction of the protective and double layer capacitances.

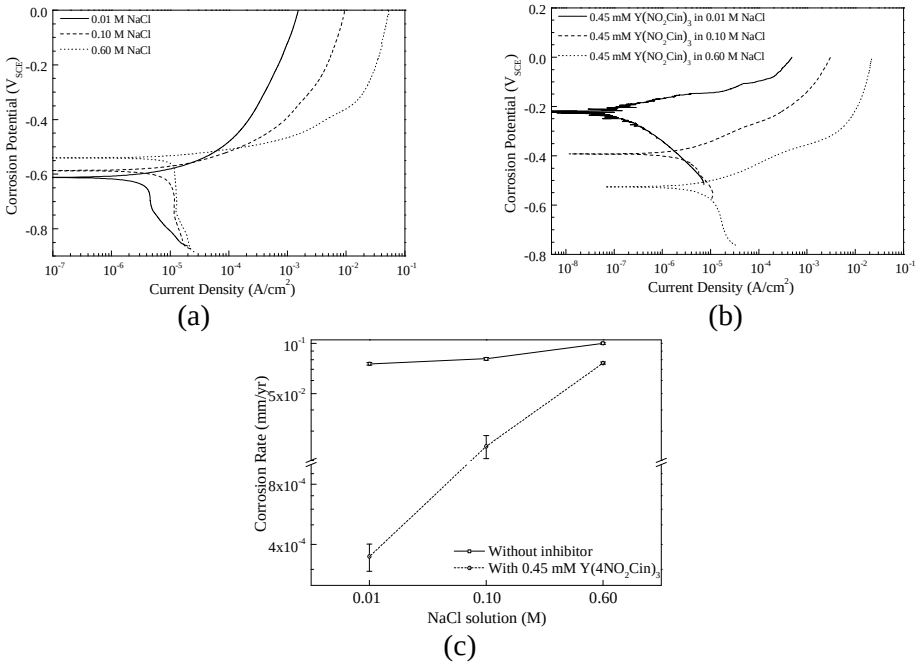

Figure 3. (a) Potentiodynamic polarization curves of mild steel immersed in: (a) different NaCl solutions and (b) 0.45 mM $Y(4NO_2Cin)_3$ solutions containing different NaCl concentrations, and (c) effect of NaCl concentration on corrosion rate of mild steel in 0.45 mM $Y(4NO_2Cin)_3$ solution.

Figure 3(a and b) shows the representative potentiodynamic polarization curves observed from steel electrodes after 10-hour elapsed for 1 cm^2 of steel immersed in different NaCl solutions and 0.45 mM $Y(4NO_2Cin)_3$ solution containing different NaCl concentrations. The results demonstrated active material behavior, indicating that a passive film was absent from the steel surfaces immersed in different NaCl solutions. However, an information of the protective layer formation was performed, when the steel surfaces immersed in 0.45 mM $Y(4NO_2Cin)_3$ solution containing different NaCl concentrations. Furthermore, higher corrosion current densities were observed on the steel specimens immersed in the NaCl solutions and the corrosion current density increased with an increase in NaCl concentration, indicating the additional aggressiveness of Cl^- ion. Addition of $Y(4NO_2Cin)_3$ strongly decreased the corrosion current density in all solutions (from 5.73, 6.51, and 8.62 $\mu A/cm^2$ for steels in 0.01, 0.10, and 0.60 M NaCl solutions without inhibitor to 0.03, 1.60, and 2.87 $\mu A/cm^2$ with 0.45 mM $Y(4NO_2Cin)_3$ solutions containing 0.01, 0.10, and 0.60 M NaCl, respectively).

Figure 3(b) also shows that in NaCl solutions containing $Y(4NO_2Cin)_3$, the inhibitor significantly influenced both the anodic and cathodic branches. Additionally, the cathodic curves indicating diffusion-limited oxygen reduction regimes were also obtained. Figure 3(c) indicates the corrosion rates determined from potentiodynamic polarization curves in Fig. 3(a and b). Corrosion rate decreased significantly when 0.45 mM $Y(4NO_2Cin)_3$ was added to solutions. In addition, increasing Cl^- ion concentration increased corrosion rate of steel in both solutions without and with 0.45 mM $Y(4NO_2Cin)_3$ addition. The corrosion rates are calculated from the corrosion current density, based on Faraday's law [22]:

$$\text{Corrosion rate (mm/yr)} = \frac{3.16\times10^8\times i_{corr}\times M}{z\times F\times\rho} \quad (1)$$

where 3.16×10^8 is the metric and time conversion factor, i_{corr} the corrosion current density (A/cm^2), M is the molar mass of the metal (g/mole), z is the number of electrons transferred per metal atom, F is Faraday's constant, and ρ is the density (g/cm^3).

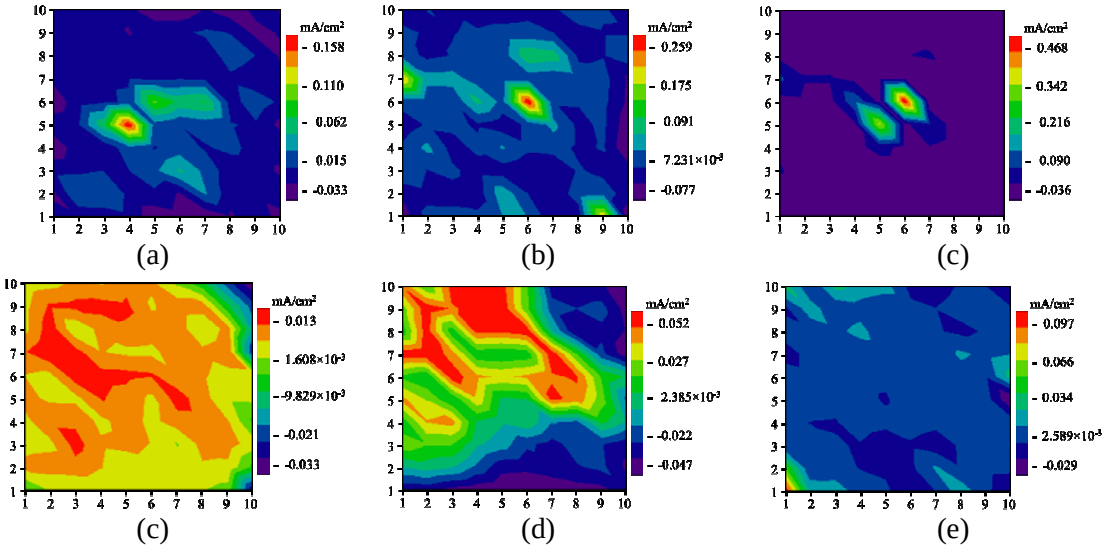

Figure 4. Galvanic current distribution maps measured over a steel WBE surface in (a) 0.01, (b) 0.10, and (c) 0.60 M NaCl solutions, and 0.45 mM $Y(4NO_2Cin)_3$ solutions containing (d) 0.01, (e) 0.10, and (f) 0.60 M NaCl.

Galvanic current as a local electrochemical parameter was determined using a wire beam electrode in NaCl solution and 0.45 mM $Y(4NO_2Cin)_3$ solutions containing different NaCl concentrations as shown in Fig. 4. The results indicated that the galvanic current distribution maps of WBE surfaces immersed in different NaCl concentration solutions without $Y(4NO_2Cin)_3$ addition in Fig. 4(a-c) showed severe corrosion due to a formation of a small number of minor anodes and major cathodes, resulting in localized corrosion. Highest corrosion could be happened at the maximum anodic current density due to a dissolution of the most active anode. The huge positive current density results in more electrons moving out from the most active anode to cathodic positions when NaCl concentration increases. Thus, pitting corrosion increased with an increase in NaCl concentration in the investigated solution. This agrees with the high rate of corrosion and pitting observed in polarization and EIS results as well as SEM results described below. Interestingly, random distribution of minor anodes and major cathodes on the WBE surface was performed when 0.45 mM $Y(4NO_2Cin)_3$ was added to solutions even with higher NaCl concentration, resulting in the degradation of small anode and large cathode phenomenon as shown in Fig. 4(d-f). Therefore, 0.45 mM $Y(4NO_2Cin)_3$ addition promotes uniform corrosion rather than localized corrosion for steel in NaCl solutions.

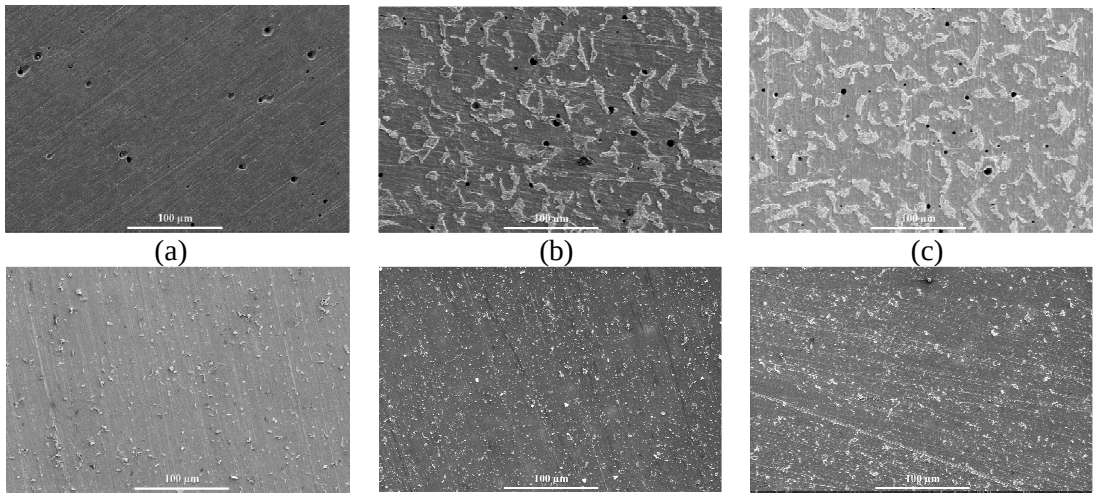

Figure 5. SEM images of mild steel surfaces after 10 h immersion in (a) 0.01, (b) 0.10, and (c) 0.60 M NaCl solutions, and 0.45 mM $Y(4NO_2Cin)_3$ solutions containing (a) 0.01, (b) 0.10, and (c) 0.60 M NaCl.

Figure 5(a-c) represents the SEM images of steel surfaces after 10 hour-immersion in different NaCl concentration solutions. It is indicated that a significant difference of surface morphologies was observed on steel surface due to the pitting corrosion. An increase in NaCl concentration was accelerated by severe corrosion due to the inward penetration of Cl^-, resulting in not only pitting corrosion but also severe corrosion attacking outside the pit when NaCl concentration increased. However, no pitting was observed on the steel surface immersed in solutions containing 0.45 mM $Y(4NO_2Cin)_3$ as shown in Fig. 5(d-f). It is suggested that $Y(4NO_2Cin)_3$ addition inhibited the localized corrosion of steel in NaCl solutions. The results in Fig. 5(d-f) also indicated that an increase of NaCl concentration in 0.45 mM $Y(4NO_2Cin)_3$ solution increased the rough level of the steel surface due to a more aggressive environment, resulting in lower inhibition efficiency obtained from electrochemical results.

Figure 6 represents the attenuated total reflectance Fourier transform infrared spectroscopy (ATR-FTIR) results of $Y(4NO_2Cin)_3$ powder as raw materials and the mild steel surfaces after

10-hour immersion in 0.45 mM $Y(4NO_2Cin)_3$ solutions containing 0.01, 0.10, and 0.60 M NaCl, respectively. Figure 6(a) describes ATR-FTIR result of raw $Y(4\text{-}NO_2Cin)_3$ powder and indicates that the $\nu(C=C)_{propenyl}$ bands of the Y^{III} 4-nitrocinnamate complexes are presented around 1651 and 1643 cm^{-1}, respectively. The Y^{III} complexes occurred at 1553 and 1420 cm^{-1} could be attributed to the $\nu_{as}(CO_2)$ and $\nu_s(CO_2)$ absorptions, respectively. While the absorptions of $Y(4\text{-}NO_2Cin)_3$ assigned to the 1512 and 1346 cm^{-1} bands correspond to the $\nu_{as}(NO_2)$ and $\nu_s(NO_2)$ [17,20]. Figure 6(b) indicates ATR-FTIR spectra of the steel surfaces after 10-hour immersion in 0.45 mM $Y(4NO_2Cin)_3$ solutions containing 0.01, 0.10, and 0.60 M NaCl, respectively. The main peaks were observed around 1651 and 1643 cm^{-1} attributed to C=C ring from propenyl group. The $\nu_{as}(CO_2)$ and $\nu_s(CO_2)$ absorptions could be assigned around 1553 and 1420 cm^{-1}. Particularly, the $\nu_{as}(NO_2)$ and $\nu_s(NO_2)$ absorptions assigned to the peaks around 1553 and 1420 cm^{-1}. The absorption peak intensities of the C=C, $\nu(CO_2)$, and $\nu(NO_2)$ absorptions on the steel surface increase with a decrease in NaCl concentration, indicating the formation of a mixed metal 4-nitrocinnamate species on the steel surface. These phenomena are attributed to the presence of the mixed metal 4-nitrocinnamate species in the protective film on the steel surface, acting as barrier layer to mitigate the general and localized corrosions. Therefore, the interaction of hydrated iron oxide/hydroxide with 4-nitrocinnamate and yttrium oxide/hydroxide precipitation on the steel surface promoted the formation of an adherent, continuous protective layer, resulting in general and localized corrosion inhibition [17-19].

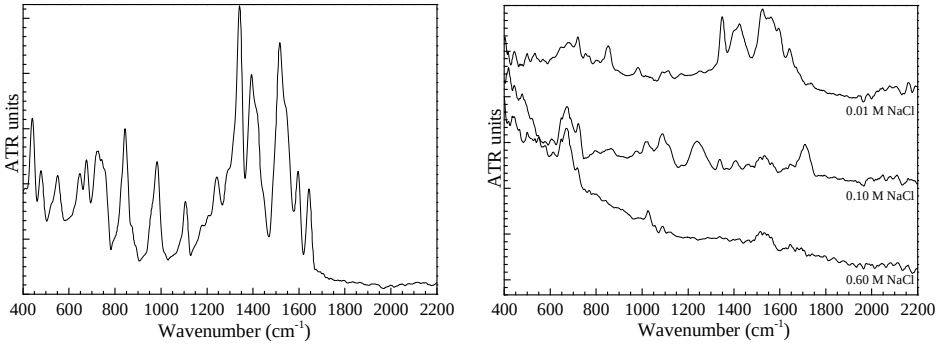

Figure 6. ATR-FTIR spectra of $Y(4NO_2Cin)_3$ powder as raw material and mild steel surface after 10-hour immersion in 0.45 mM $Y(4NO_2Cin)_3$ solutions containing (a) 0.01, (b) 0.10, and (c) 0.60 M NaCl.

4. CONCLUSIONS

This paper mainly reports the advantage of the $Y(4NO_2Cin)_3$ compound to perform highly efficient inhibitor suitable for mitigating corrosion and localized corrosion of mild steel in an aggressive chloride environment. The results indicated that corrosion rate of mild steel increased with an increase in Cl^- ion in aggressive solutions due to lower corrosion current density, corrosion product and charge transfer resistances, as well as higher pitting corrosion. Fortunately, the severe corrosion has been prevented by the addition of $Y(4NO_2Cin)_3$ compound to the aggressive chloride solutions due to the formation of an evidence protective film via the bonding on the $Y(4NO_2Cin)_3$ molecules onto the mild steel surface. The $Y(4NO_2Cin)_3$ compound showed an increased inhibition performance for mild steel in aggressive solution containing lower Cl^- ion concentration due to the formation of a protective film layer on the mild steel surface. Surface analysis also indicated that the formation of bimetallic and 4-nitrocinnamate compounds as a barrier layer on the steel surface because of cooperative adsorption of ionic species with

chemisorbed molecular NO_2^- and COO^-, as well as Y^{3+} hydrolysis on the neighboring adsorption sites for the mild steel immersed in solution containing lower Cl^- ion concentration. Furthermore, EIS showed that $Y(4NO_2Cin)_3$ compound added to solution increased the protective and charge transfer resistances with a decrease in Cl^- ion concentration in the investigated solutions. Interestingly, the WBE results indicated that the $Y(4NO_2Cin)_3$ compound promoted uniform corrosion rather than localized corrosion, suggesting localized corrosion inhibition, which plays a very important role in corrosion protection. In addition, the study also suggested that an excellent agreement was observed among the surface analysis, electrochemical and WBE results for evaluating the performance of corrosion and localized corrosion inhibition.

Acknowledgement. This research is funded by Vietnam National Foundation for Science and Technology Development (NAFOSTED) under grant number 104.06-2016.08. The author is also grateful for the support of Vietnam Oil & Gas Group and PetroVietnam University. We are also grateful to Mahesh Vaka from the Science Engineering Health, RMIT University for his thorough editorial work and discussions.

REFERENCES

1. Stoddard B. C. - Steel: From mine to mill, the metal that made America, Motorbooks International, 2015.
2. Cole I. S. - The science of pipe corrosion: A review of the literature on the corrosion of ferrous metals in soils, Corros. Sci. **56** (2012) 5-16.
3. Panossian Z., de Almeida N. L., de Sousa R. M. F., de Souza Pimenta G., Marques L. B. S. - Corrosion of carbon steel pipes and tanks by concentrated sulfuric acid: A review, Corros. Sci. **58** (2012) 1-11.
4. Nam N. D., Lee D. Y., Kim J. G., Park N. J. - Effect of cold rolling on the corrosion properties of low-alloy steel in an acid-chloride solution, Met. Mater. Int. **20** (2014) 469-474.
5. da Silva F. S., Bedoya J., Dosta S., Cinca N., Cano I. G., Guilemany J. M., Benedetti A.V. - Corrosion characteristics of cold gas spray coatings of reinforced aluminum deposited onto carbon steet, Corros. Sci. **114** (2017) 57-71.
6. Parhizkar N., Shahrabi T., Ramezanzadeh B. - A new approach for enhancement of the corrosion protection properties and interfacial adhesion bonds between the epoxy coating and steel substrate through surface treatment by covalently modified amino functionalized graphene oxide film, Corros. Sci. **123** (2017) 55-75.
7. Nam N. D., Kim M. J., Kim J. G. - Corrosion behavior of low alloy steels containing manganese in mixed chloride sulfate solution, Metall. Mater. Trans. A **45** (2014) 893-905.
8. Jevremović I., Singer M., Nešić S., Stanković V. M. - Inhibition properties of self-assembled corrosion inhibitor talloil diethylenetriamine imidazoline for mild steel corrosion in chloride solution saturated with carbon dioxide, Corros. Sci. **77** (2013) 265-272.
9. Somers A. E., Deacon G. B., Hinton B. R. W., MacFarlane D. R., Junk P.C., Tan M. Y. J., Forsyth M. - Recent developments in environment-friendly corrosion inhibitors for mild steel, J. Indian Inst. Sci. **96** (2016) 285-292.
10. Maria F., Bruce H. - Rare earth-based corrosion inhibitors, Elsevier, 2014.
11. Nam N. D., Somers A., Mathesh M., Seter M., Hinton B., Forsyth M., Tan M. Y. J. - The

behaviour of praseodymium 4-hydroxycinnamate as an inhibitor for carbon dioxide corrosion and oxygen corrosion of steel in NaCl solutions, Corros. Sci. **80** (2014) 128-138.

12. Nam N. D., Panaitescu C., Tan M. Y. J., Forsyth M., - Hinton B. An interaction between praseodymium 4-hydroxycinnamate with AS1020 and X65 steel microstructures in carbon dioxide environment, J. Electrochem. Soc. **165** (2018) C50-C59.
13. Nam N. D., Bui Q. V., Mathesh M., Tan M. Y. J., Forsyth M. - A study of 4-carboxyphenylboronic acid as a corrosion inhibitor for steel in carbon dioxide containing environments, Corros. Sci. **76** (2013) 257-266.
14. Katz S. A., Salem H. - The toxicology of chromium with respect to its chemical speciation: a review, J. Appl. Toxicol. **13** (1993) 217-224.
15. Burg R. V., Liu D. - Chromium and hexavalent chromium, J. Appl. Toxicol. **13** (1993) 225-230.
16. Tan Y. J. - Organic molecules showing the characteristics of localized corrosion aggravation and inhibition, Corros. Sci. **53** (2011) 2041-2045.
17. Hien P. V., Vu N. S. H., Thu V. T. H., Somers A., Nam N. D. - Study of yttrium 4-nitrocinnamate to promote surface interactions with AS1020 steel, Appl. Surf. Sci. **412** (2017) 464-474.
18. Nam N. D., Thang V. Q., Hoai N. T., Hien P. V. - Yttrium 3-(4-nitrophenyl)-2-propenoate used as inhibitor against copper alloy corrosion in 0.1 M NaCl solution, Corros. Sci. **121** (2016) 451-461.
19. Nam N. D., Hung T. V., Ngan D. T., Hung N. L. T., Hoi T. K. N. - Film formation in $Y(4NO_2Cin)_3$ compound on 6061 aluminum alloy to protect against corrosion in chloride ion media, J. Taiwan Inst. Chem. Eng. **67** (2016) 495-504.
20. Deacon G. B., Forsyth M., Junk P. C., Leary S. G., Lee W. - Synthesis and characterisation of rare earth complexes supported by para-substitutedcinnamate ligands, Z. Anorg. Allg. Chem **635** (2009) 833-839.
21. Barsoukov E., Macdonald J. R. - Impedance spectroscopy theory, experiment, and applications, 2005.
22. Jonse D. A. - Principles and Prevention of Corrosion, Second ed., Prentice-Hall, New Jersey, 1996.